



HAL
open science

Seismic internal stability of saturated reinforced soil retaining walls using the upper bound theorem of limit analysis

Hicham Alhajj Chehade, Daniel Dias, Marwan Sadek, Oriane Jenck, Fadi Hage Chehade

► To cite this version:

Hicham Alhajj Chehade, Daniel Dias, Marwan Sadek, Oriane Jenck, Fadi Hage Chehade. Seismic internal stability of saturated reinforced soil retaining walls using the upper bound theorem of limit analysis. *Soil Dynamics and Earthquake Engineering*, 2022, 155, pp.107180. 10.1016/j.soildyn.2022.107180 . hal-03929847

HAL Id: hal-03929847

<https://hal.science/hal-03929847v1>

Submitted on 22 Jul 2024

HAL is a multi-disciplinary open access archive for the deposit and dissemination of scientific research documents, whether they are published or not. The documents may come from teaching and research institutions in France or abroad, or from public or private research centers.

L'archive ouverte pluridisciplinaire **HAL**, est destinée au dépôt et à la diffusion de documents scientifiques de niveau recherche, publiés ou non, émanant des établissements d'enseignement et de recherche français ou étrangers, des laboratoires publics ou privés.



Distributed under a Creative Commons Attribution - NonCommercial 4.0 International License

26 **Consent to participate:** Not applicable
27 **Consent for publication:** Not applicable
28 **Availability of data and material:** Not applicable
29 **Code availability:** Not applicable

30

31 **Acknowledgements**

32 The research team thanks the Lebanese University for partially funding this work.

33 **Abstract.** This study concerns the seismic internal stability analysis of saturated reinforced soil retaining walls using
34 the discretization technique and the limit analysis upper bound approach. The discretization technique permits to
35 generate the potential failure mechanism of reinforced structures point by point. The seismic forces are represented
36 based on the pseudo-dynamic approach. This latter is more realistic than the pseudo-static one which is commonly used.
37 It allows accounting for the dynamic characteristics of the seismic loading. Knowing that the water presence is the main
38 cause of most failure cases reported in the literature, the pore water effect within the backfill soil is considered together
39 with a possible crack opening in cohesive soils. The reinforcement strength required to prevent the saturated reinforced
40 soil wall failure is obtained through an optimization process. The developed approach is validated by comparison with
41 the existing results obtained by Abd and Utili (2017) using the conventional limit analysis method. The presence of
42 pore-water pressure leads to an increase in the reinforcement strength required to prevent the failure. Discussions are
43 then carried out to point out the effects of the crack presence, the seismic loading and the soil properties on the structure
44 stability. The cases of non-homogeneous and layered soils are investigated.

45

46 **Keywords:** Reinforced soil, Pore water effect, Limit analysis, Discretization technique, Pseudo-dynamic approach.

47 **1 Introduction**

48 Geosynthetic reinforced soil retaining walls are now a mature technology. They are structures which allow
49 reinforcing a compacted backfill with horizontal reinforcement elements connected to the wall facing. The
50 reinforcements significantly improve the global shear strength. The success of these structures is mainly due to their
51 advantages compared to conventional retaining walls, concerning cost, time and space saving, in addition to their good
52 performance due to their flexibility during strong earthquakes.

53 A compacted cohesionless granular soil is recommended as a backfill in the reinforced zone by most design codes
54 (e.g., FHWA, NF P 94-270). The use of a good drainage system is also required. These requirements avoid the

55 development of interstitial pore pressures in the reinforced zone. However, the use of geosynthetic reinforcements,
56 which do not have corrosion risk that can affect the metallic reinforcements, gives the opportunity to use poorly
57 draining cohesive soils when granular soils are not available or are expensive (Guler et al. 2007). This soil type was
58 successfully used in the reinforced earth wall construction (Ricchio et al. 2014). Nevertheless, the use of these soils can
59 lead to several problematical issues and therefore, reduce the system stability (Abd and Utili 2017). Among these
60 problems, the pore-water pressures development and the crack formation in the backfill zone are the most dangerous
61 ones. Koerner and Koerner (2018) presented 320 geosynthetic reinforced mechanically stabilized earth walls failure
62 cases. They reported that the reinforced backfill soils used in 73% of these cases were cohesive ones. In addition, they
63 reported that pore pressures developed in the reinforced backfill caused the failures of 63% of these walls.

64 The water presence in the cohesive backfill must be addressed due to its low permeability and the possible
65 malfunction of the drainage system that could be caused by its clogging by fines. The system shear strength can then be
66 significantly reduced. Furthermore, the cohesive soils present limited tensile strengths, and therefore, they can develop
67 cracks on soil surface (Abd and Utili 2017). The cracks formation affects the reinforced cohesive soil retaining walls
68 stability (Alhajj Chehade et al., 2019). This phenomenon has been observed at the surface of many reinforced cohesive
69 slopes after earthquake events (Ling et al. 2001) in addition to the experimental studies (Porbaha and Goodings 1996).

70 The assessment of the seismic stability of reinforced soil structures could be performed using numerical approaches
71 (finite differences-finite elements), limit equilibrium and limit analysis methods. The cracks introduce a discontinuity in
72 the static and kinematic fields which induces a computationally-expensive cost to consider these discrete discontinuities
73 in numerical methods (Utili and Abd 2016). Hence, to conduct a parametric study on the reinforced backfill retaining
74 wall stability considering cracks formation, the use of numerical methods requires complex development. The most
75 commonly used method to assess the unreinforced and reinforced slopes stability considering the cracks presence, in the
76 literature, is the limit equilibrium one (Baker 1981; Chowdhury and Zhang 1991; Baker and Leshchinsky 2001, 2003).
77 However, only the pre-existing crack case is considered through this method by the modification of the failure surface
78 geometry. Alternatively, Chen et al. (1969) developed an efficient method to analyze slopes stability, known as the limit
79 analysis method. Since then, this method has been used to assess the stability of all geotechnical structures including the
80 reinforced soil walls. It permits to obtain more rigorous solutions considering the stress-strain relation of soils than the
81 limit equilibrium does. In addition, it permits to include the process of crack propagation as a part of the failure
82 mechanism. Recently, many studies assessed unreinforced slopes stability considering the cracks presence using the
83 limit analysis upper bound approach (Michalowski 2013; Utili 2013; Zhao et al. 2016). In addition, Abd and Utili
84 (2017) first investigated the effect of cracks on the stability of geosynthetic reinforced slopes. A homogeneous backfill
85 soil was considered and two cracks types are examined, pre-existing cracks and cracks that can be formed as a part of
86 the collapse mechanism.

87 In the reinforced soil wall stability analysis, a rotational toe log-spiral failure surface is generally considered as the
88 most critical failure mechanism (Abd and Utili 2017; Alhaji Chehade et al. 2019, 2020). Mollon et al. (2011) developed
89 a discretization method coupled with the kinematic approach of limit analysis, in the framework of face stability
90 assessment of circular tunnels. The discretization technique permits to overcome the conventional kinematic approach
91 limitations by generating the failure mechanism point by point. It allows the consideration of non-uniform soils and the
92 use of the pseudo-dynamic approach to represent the seismic loading instead of the pseudo-static one, which is more
93 realistic. The good agreement of the results with the field measurements in the work of Mollon et al. (2011), inspired
94 many researchers to extend the discretization-based kinematic analysis to assess the stability of different geotechnical
95 structures (Pan and Dias 2015; Qin and Chian 2018; Sun et al. 2018). In this context, Alhaji Chehade et al. (2019)
96 successfully extended it to generate a toe log-spiral failure mechanism in the framework of reinforced soil walls
97 stability assessment.

98 In this study, the limit analysis upper bound theorem is employed for the seismic stability assessment of
99 geosynthetic reinforced soil retaining walls with saturated non-uniform backfill soils. A rotational failure mechanism
100 generated point by point through the discretization technique is considered. This technique gives the possibility to
101 represent the seismic loading through the pseudo-dynamic approach as well as the possibility of considering non-
102 homogeneous backfill soil. A saturated cohesive backfill soil is considered. The influences of the pore water pressure,
103 the cracks presence, the soil heterogeneity and the seismic loading on the seismic internal stability of reinforced soil
104 retaining walls are assessed and discussed.

105 **2 Upper bound theorem of limit analysis**

106 The upper bound theorem of limit analysis is based on the balance between the internal and external forces of a
107 kinematically admissible velocity field. An advantage of this method is the consideration of the soil stress-strain
108 relationship through the concept of yield criterion and its associated flow rule. Nevertheless, among the disadvantages of
109 this method is that the shape of the failure surface is imposed. In addition, the soil behavior is assumed to be an ideal
110 rigid, perfectly plastic body with an associated normality rule based on the Coulomb yield condition, which is not
111 rational.

112 In this study, the kinematic theorem is applied to analyze the seismic internal stability of geosynthetic reinforced
113 soil retaining walls in saturated poorly draining backfills. A rigid block assumption is considered and the soil is
114 considered as an ideal rigid perfectly plastic material obeying associated flow rule. This theorem gives a rigorous lower
115 bound to the required reinforcement tensile strength that prevents the failure of the reinforced soil walls. The reinforced
116 wall fails if the external work rate exceeds the internal energy dissipation rate for any assumed kinematically admissible
117 failure mechanism. A rotational log-spiral failure mechanism passing through the wall toe is assumed (Abd and Utili

118 2017; Alhadj Chehade et al. 2019a, 2020). The geosynthetic reinforcements only resist tension without any bending or
119 compression resistance. These reinforcements are finite in number, having a uniform length, placed with a uniform
120 vertical spacing, providing therefore a uniform tensile strength distribution over depth. They are placed horizontally and
121 provide forces that correspond to their tensile strength or pullout resistance.

122 3 Discretization technique

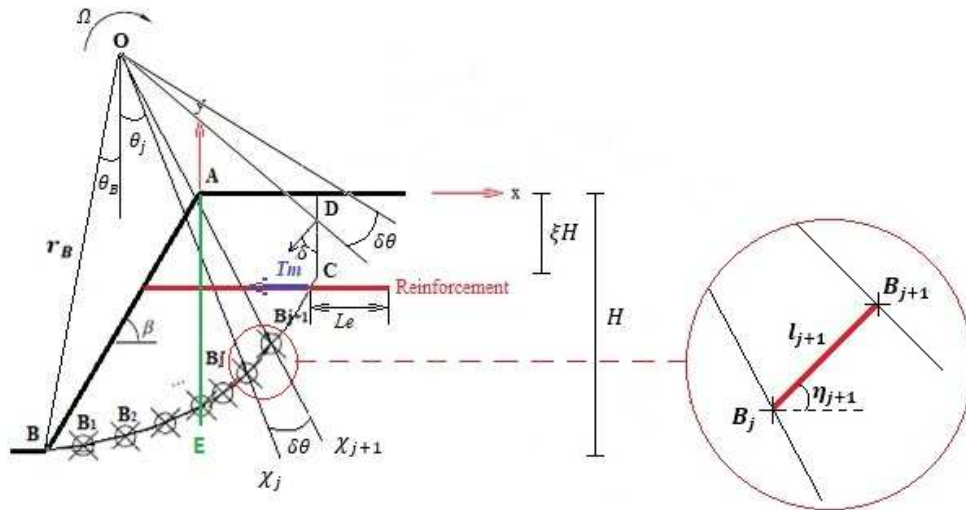
123 The discretization technique was proposed for the first time by Mollon et al. (2011) to generate a rotational failure
124 mechanism, in the framework of the stability analysis of circular tunnels. Alhadj Chehade et al. (2019) extended this
125 technique for reinforced soil retaining walls stability assessment. It allows to overcome the limitations of the traditional
126 kinematic approach which can only be used in case of homogeneous soils and can only represents the seismic loading
127 by the pseudo-static approach (Alhadj Chehade et al., 2019). This is because when the sliding surface is generated point-
128 by-point through this technique, the soil properties and the seismic loading could be easily specified for each
129 infinitesimal part of the failure surface. In this paper, a log-spiral failure mechanism passing by the wall toe is generated
130 using this technique as illustrated in Fig. 1. A level backfill is considered (Horizontal surface), H denotes the wall
131 height and β is the angle formed between the horizontal and the wall facing.

132 The failure surface $ABCD$ delimits the moving soil area and the soil at rest. It is formed by the log-spiral surface BC
133 and the potential formed crack CD . Along the first surface, the soil fails purely in shear while it can also fail in tension
134 along the crack. The failure surface is defined by the parameters r_B , θ_B and ξ . r_B corresponds to the length of OB , θ_B
135 corresponds to the angle between the vertical direction and the (OB) and ξ is the ratio of the crack depth to the wall
136 height. Two cracks' cases can be involved in the failure mechanism. Pre-existing cracks in the reinforced soil due to
137 weathering, desiccation and other climate phenomenon, and cracks that are formed during the collapse mechanism
138 process. For simplicity in this study and similar to various studies (Michalowski 2013; Utili 2013; Zhao et al. 2016), the
139 cracks considered are assumed to be vertical even though they can presented curved shapes as reported by Hu et al.
140 (2010). For rigid blocks assumption, the soil block $ABCD$ is rotating about the center O with an angular velocity Ω . The
141 center of rotation O can be defined by the mechanism parameters r_B and θ_B . The discretization technique aims at
142 defining the failure surface by a series of points B_j iteratively i.e. each point is derived from the previous point,
143 knowing that the wall toe is the starting point of the generation process. The normality condition should be respected in
144 order to obtain a kinematically admissible failure mechanism. Therefore, the angle between each segment $[B_j B_{j+1}]$
145 formed by two consecutive points on the failure surface, and the velocity vector should be equal to the soil friction
146 angle φ_i . This angle becomes equal to δ along the vertical crack CD as depicted in Fig.2. The angle $\delta\theta$, known as the
147 discretization angle, denotes the angle between two consecutives radial lines, χ_j and χ_{j+1} . The accuracy of the failure

148 mechanism is affected by this angle. A closer match to the log-spiral failure mechanism is obtained with small values of
 149 this angle. The detailed steps and equations used to generate the failure mechanism are presented in (Alhajj Chehade et
 150 al., 2019).

151

152



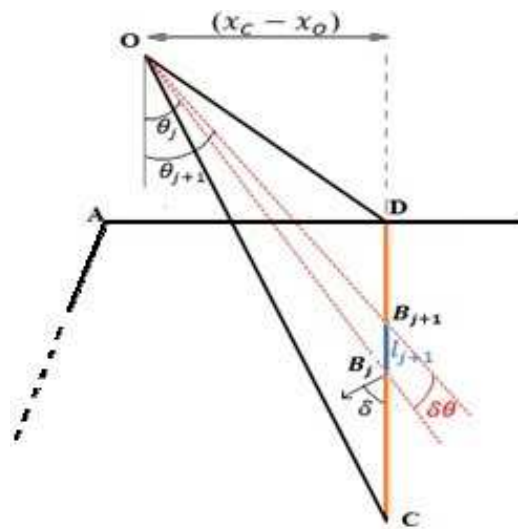
153

154

Fig.1. Generation of the potential failure surface by the discretization technique

155

156



157

158

159

Fig.2. Generation of the crack

160 4 Pseudo-dynamic approach

161 The use of the real-time acceleration history to represent a seismic event is always the best choice. Such approach
 162 requires a high computational effort using numerical analysis. However, the seismic loading is commonly represented

163 using the pseudo-static approach when the former approach is not justifiable. In the framework of this approach, the
 164 seismic accelerations are considered constants. Alternatively, Steedman and Zeng (1990) proposed a more realistic
 165 approach, the pseudo-dynamic one, to represent the seismic loading through the limit equilibrium method. It represents
 166 a good compromise between the pseudo-static accelerations and the real-time acceleration history. It accounts for the
 167 time and spatial variation of the seismic shaking. The discretization method allows the use of this approach with the
 168 kinematic theorem of limit analysis to represent the seismic loading which is not applicable in case of conventional
 169 limit analysis method (Qin and Chian 2017, 2019).

170 The pseudo-dynamic analysis considers finite shear and primary wave velocities acting within soil medium, while
 171 the pseudo-static one assumes infinite values. The soil shear modulus G is assumed to remain constant during the
 172 shaking in the whole soil medium. This means that the shear wave velocity V_s and the primary wave velocity V_p that
 173 depend on G , remain also constant. On the other hand, the accelerations magnitudes and phases vary in both directions
 174 along the backfill depth. The ratio $V_p/V_s = 1.87$, used for soils characterized with a Poisson's ratio $\nu = 0.3$, is
 175 considered in this paper.

176 In reality, as mentioned before, the real time history acceleration with a wide frequency content is the best way to
 177 consider an earthquake. For simplicity, similar to most previous studies (Choudhury and Nimbalkar, 2006; Nimbalkar
 178 et al. 2006; Ahmad and Choudhury 2008; Basha and Sivakumar Babu 2011; Qin and Chian 2017, 2019; Alhadjj Chehade
 179 et al. 2019a, 2020), this work adopt a sinusoidal acceleration. The accelerations magnitudes in both directions are
 180 assumed to vary linearly along the reinforced backfill depth. If the accelerations are amplified by a factor f at the
 181 ground surface related to the accelerations at the wall base, the horizontal and vertical acceleration expressions at any
 182 depth y and time t can be expressed as:

$$183 \quad \begin{cases} a_h = \left[f + \frac{y}{H}(f - 1) \right] \cdot k_h g \sin \frac{2\pi}{T} \left(t - \frac{H + y}{V_s} \right) \\ a_v = \left[f + \frac{y}{H}(f - 1) \right] \cdot k_v g \sin \frac{2\pi}{T} \left(t - \frac{H + y}{V_p} \right) \end{cases} \quad (1)$$

184 where H is the wall height, g the acceleration due to gravity, T the lateral and vertical shakings period, k_h and k_v the
 185 horizontal and vertical seismic coefficients respectively.

186 **5 Discretization-based kinematic analysis**

187 The limit analysis kinematic approach is based on the balance between internal energy dissipation \dot{D} , and the work
 188 rates of the external forces, \dot{W} , in any kinematically admissible failure mechanism. Its application gives a lower bound
 189 to the required tensile reinforcement strength T_m , which ensures the reinforced soil wall stability.

190 The internal energy dissipation during the failure process takes place in the geosynthetic reinforcing elements by
 191 tensile failure or/and along the reinforcing elements by pullout failure. In addition, based on the rigid blocks
 192 assumption, an internal energy is dissipated along the discontinuity surface due to the soil plastic deformation. When
 193 the failure mechanism involves the cracks presence, the internal energy dissipation along the crack CD must be
 194 accounted only in the case of crack that forms during the failure mechanism process since an amount of energy is
 195 required for its formation (Michalowski, 2013). On the other hand, for a pre-existing crack that is already present in the
 196 soil, $\dot{D}_{CD}=0$.

197 On the other hand, the external work rates involve the soil block weight $ABCD$ work rate, the inertia forces work
 198 rates representing the seismic loading in both directions and the pore water pressure one.

199 The required tensile reinforcement strength to maintain the reinforced soil wall equilibrium, can be determined by
 200 equating the external work rates and the internal energy dissipations, as stated by the kinematic theorem of limit
 201 analysis. This approach provides a lower bound for the required strength through an optimization procedure. The
 202 energy balance equation is given by:

$$203 \quad \dot{W}_\gamma + \dot{W}_{kh} + \dot{W}_{kv} + \dot{W}_u = \dot{D}_{BC} + \dot{D}_{CD} + \dot{D}_T \quad (2)$$

204 Where \dot{W}_γ is the soil weight work rate ; \dot{W}_{kh} and \dot{W}_{kv} are the seismic forces work rates ; \dot{W}_u is the pore-water pressure
 205 work rate; \dot{D}_{BC} , \dot{D}_{CD} and \dot{D}_T are the internal energy dissipated along the rotational part of the sliding surface, along the
 206 vertical crack and, in and along the reinforcements respectively.

207 Due to the discretization, the computations of the external work rates are performed by summation of the elementary
 208 work rates of the elementary trapezoidal surface $B'_j B_j B'_{j+1} B_{j+1}$ shown in Fig. 3 and are expressed as:

$$209 \quad \dot{W}_\gamma = \sum_j (\gamma \cdot A_j) \cdot (\Omega \cdot (x_{Gj} - x_o)) \quad (3)$$

$$210 \quad \dot{W}_{kh} = \sum_j \left(\gamma \cdot A_j \cdot \left[f + \frac{y_{Gj}}{H} (f - 1) \right] \cdot k_h \sin \frac{2\pi}{T} \left(t - \frac{H + y_{Gj}}{V_s} \right) \right) \cdot (\Omega \cdot (y_o - y_{Gj})) \quad (4)$$

$$211 \quad \dot{W}_{kv} = \sum_j \left(\gamma \cdot A_j \cdot \left[f + \frac{y_{Gj}}{H} (f - 1) \right] \cdot k_v \sin \frac{2\pi}{T} \left(t - \frac{H + y_{Gj}}{V_p} \right) \right) \cdot (\Omega \cdot (x_{Gj} - x_o)) \quad (5)$$

212
 213
 214 where A_j is the infinitesimal area of the trapezoidal element $B'_j B_j B'_{j+1} B_{j+1}$; x_{Gj} and y_{Gj} are the coordinates of its
 215 gravity center G_i ; x_o and y_o are the center of rotation coordinates of the rotational failure mechanism O .
 216

241 The first term in Eq. (7) is assumed to be zero since a rigid block is considered. In the framework of the failure
 242 surface generation using the point-to-point method, the kinematical admissibility condition must be satisfied and
 243 therefore, the velocity vector must be inclined by to the failure surface by an angle equal the soil friction angle φ .
 244 Hence the angle between the vector n_i and the velocity vector is equal to $\frac{\pi}{2} + \varphi$. The velocity vector of the collapse
 245 block at a point B_j of the failure surface is equal to the product of the angular velocity Ω by the length of $[OB_j]$, L_j . The
 246 pore-water pressure work rate along the failure surface is then given by the summation of elementary work rates as
 247 follows:

$$248 \quad \left\{ \begin{array}{ll} \dot{W}_u = \sum_j r_u \cdot \gamma \cdot (x_j \cdot \tan \beta - y_j) \cdot l_j \cdot \Omega \cdot L_j \cdot \sin \varphi & \text{along the boundary surface } BE \\ \dot{W}_u = \sum_j r_u \cdot \gamma \cdot (-y_j) \cdot l_j \cdot \Omega \cdot L_j \cdot \sin \varphi & \text{along the boundary surface } ED \end{array} \right. \quad (8)$$

249 where x_j and y_j are the coordinates of point B_j and l_j is the length of $[B_{j-1}B_j]$.

250 Since rigid blocks assumption is considered, the internal energy dissipation occurs along the sliding surface that
 251 separates the failure region and the soil at rest, and along the reinforcements. The internal energy dissipated along the
 252 sliding surface is divided into two parts: along the log-spiral part and along the vertical crack. Eq. 9 gives the
 253 expression of \dot{D}_{BC} , as a summation of the internal work rate per infinitesimal length as follows:

$$254 \quad \dot{D}_{BC} = \sum (c_j \cdot (L_j \cdot \Omega \cdot \cos \varphi_j) \cdot l_j) \quad (9)$$

255 Where L_j and l_j are respectively the lengths of the segments $[OB_j]$ and $[B_{j-1}B_j]$, c_j and φ_j are respectively the soil
 256 cohesion and the soil friction angle at the point B_j .

257 Eq. 10 gives the internal energy dissipation along the vertical crack CD for soil tensile cut-off (zero tensile strength)
 258 which is generally assumed for safety reasons. On the other hand, Eq. 11 gives the energy dissipated in the
 259 reinforcement \dot{D}_T due to its tensile failure.

$$260 \quad \left\{ \begin{array}{ll} \dot{D}_{CD} = \sum c_j \Omega L_j \cos \varphi_j \frac{1 - \sin \delta_j}{1 - \sin \varphi_j} l_j & \text{Crack formation (tension cut - off)} \\ \dot{D}_{CD} = 0 & \text{Pre - existing crack} \end{array} \right. \quad (10)$$

261

262

$$263 \quad \left\{ \begin{array}{ll} \dot{D}_T = \sum \left(\frac{n_r T_t}{H} \cdot l_j \cdot \sin \eta_j \cdot \Omega \cdot L_j \cdot \cos(\theta_B + j \cdot \delta \theta) \right) & \text{along the boundary BC} \\ \dot{D}_T = \sum \left(\frac{n_r T_t}{H} \cdot l_j \cdot \Omega \cdot L_j \cdot \cos(\theta_B + j \cdot \delta \theta) \right) & \text{along the vertical crack CD} \end{array} \right. \quad (11)$$

264

265 where η_j is the angle that forms $[B_{j-1}B_j]$ with the horizontal axis, δ_j is the angle between the vertical crack CD and the
 266 velocity vector, T_t is the reinforcement tensile strength and n_r is the reinforcement layers number.

267 In most previous studies, the required reinforcement strength is calculated considering only this reinforcement
 268 failure type. Concerning the reinforcement length, it is determined through an optimization process in a such a way that
 269 when considering the combined failure mode (rupture in some reinforcement layers and pullout in the others), the
 270 required reinforcement strength remains the same as obtained previously when considering only the tensile failure
 271 mode. However, this method can lead to unpractical reinforcement lengths in many cases. Alhadj Chehade et al. (2019,
 272 2020) consider for the first time the combined reinforcement failures modes (tensile and pullout failures)
 273 simultaneously, with a pre-fixed reinforcement length. The internal energy dissipated along a single reinforcement due
 274 to pullout failure mode, is expressed as:

$$275 \quad d\dot{D}_p = T_p \Omega Y_i \quad (12)$$

276 where T_p is the pullout resistance of the considered reinforcement layer, Y_i is the vertical distance between the
 277 geosynthetic layer and the rotation center O .

278 Note that the pullout force calculation for the internal energy dissipation along the reinforcements, should account
 279 for the water presence. It can then be written as:

$$280 \quad T_p = 2\gamma z^*(1 - r_u)L_e f^* \quad (13)$$

281 where z^* is the overburden depth; L_e is the length of the reinforcement beyond the failure surface, known as the
 282 effective length; f^* is the apparent friction coefficient at the soil/reinforcement interface.

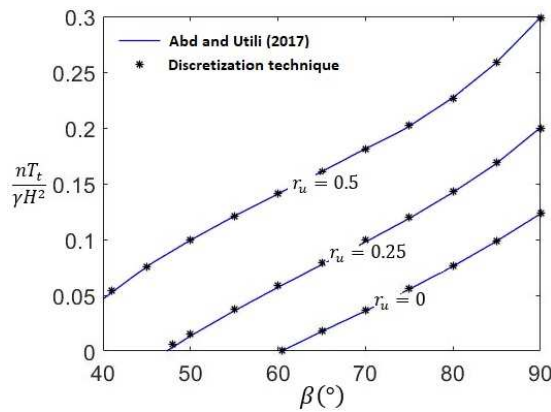
283 A lower bound to the required reinforcement is determined using a two-step genetic algorithm proposed by Guo et
 284 al. (2018) to perform an optimization process with respect to four variables, namely $[r_B, \theta_B, \xi, t]$. The length of $[OB]$,
 285 r_B , the angle between (OB) and the vertical direction, θ_B , and the normalized crack depth, ξ , are the geometrical
 286 parameters that define the failure surface (Fig.1a), while t is the time involved in the pseudo-dynamic approach. The
 287 interested readers are referred to Guo et al. (2018) for detailed description of the two-step genetic algorithm.

288 **6 Comparison with the existing solutions**

289 In order to validate the robustness of the proposed discretization mechanism, the obtained results are compared with
 290 those by Abd and Utili (2017) obtained using the conventional limit analysis method. Abd and Utili (2017) used the
 291 conventional upper bound approach of limit analysis in order to evaluate the reinforcement strength required to ensure
 292 the internal stability of geosynthetic reinforced slopes under static conditions. The effect of pre-existing crack is
 293 investigated. Only the reinforcement tensile failure is considered to determine the reinforcement strength while the

294 reinforcement length is calculated in such a way that the required reinforcement strength do not need to be increased
 295 when considering reinforcement tensile and pullout failures. They assumed both linear (uniform) and triangular
 296 reinforcement distribution. The pore water pressure effect on the required reinforcement tensile strength was analyzed
 297 by considering the same approach used here through the so-called pore-water pressure coefficient r_u .

298 In order to validate the application of the discretization method in this study, the results of the discrete method are
 299 obtained under the same conditions used in the work of Abd and Utili (2017). The case of the crack that is formed as a
 300 part of the failure mechanism is considered. The soil is considered without tensile strength (tension cut-off). The
 301 comparisons of results are depicted in Fig. 4. for different walls inclinations β , and coefficients r_u . The good agreement
 302 between the two methods shows the efficiency of the proposed method.



303
 304 **Fig. 4.** Comparison of the conventional limit analysis and the discretization technique ($\varphi = 20^\circ$ and $c/\gamma H = 0.1$)

305 **7 Numerical results**

306 *7.1 Required reinforcement strength for reinforced homogeneous soil retaining wall*

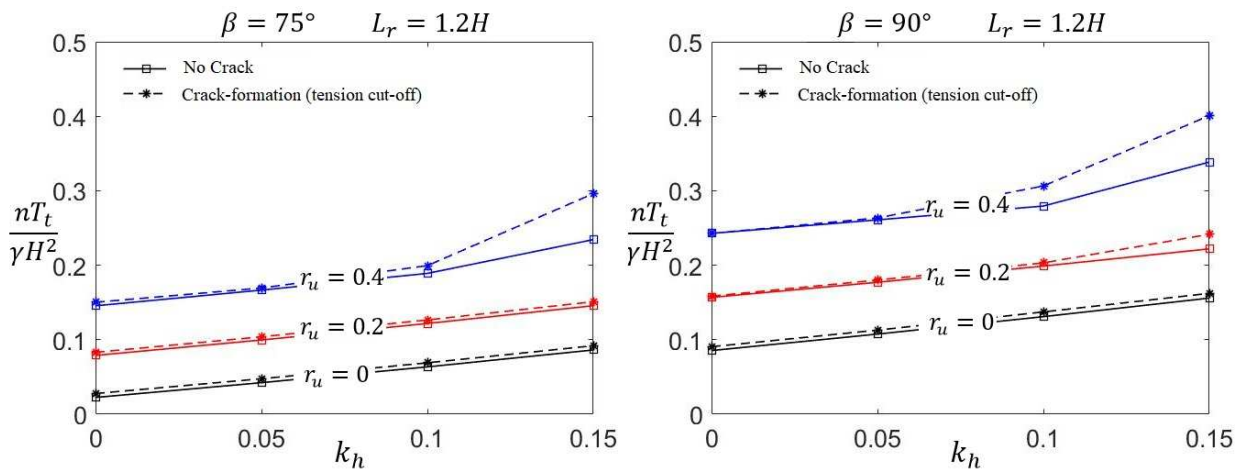
307 To investigate the pore-water pressure effect, tension crack and seismic loading, the results in terms of required
 308 reinforcement strength in a normalized form are presented for two wall inclinations $\beta = 75^\circ$ and $\beta = 90^\circ$. The two
 309 reinforcement failures modes are considered simultaneously. The following parameters are considered: $H=7\text{ m}$,
 310 $\gamma=18\text{ kN/m}^3$, $\varphi=25^\circ$, $c=12.6\text{ kPa}$, $\lambda=0.5$, $L_r=1.2\text{ H}$, $n_r=10$, $f_0^*=1.2$, $f_1^*=0.6$, $f=1.2$, $V_s=150\text{ m/s}$, $V_p=280.5\text{ m/s}$,
 311 and $T=0.3\text{ s}$, where $\lambda=k_v/k_h$, c the soil cohesion, L_r the reinforcement length, n the reinforcement number, f_0^* and f_1^*
 312 are the initial and the minimum apparent friction coefficients at the soil/strip interface.. The discretization angle $\delta\theta$ is
 313 considered to be equal to 0.01° in this paper, since this value represents a good compromise between accuracy and time
 314 calculation according to Alhajj Chehade et al. (2021).

315 According to fig. 5, it is observed that the required reinforcement strength increases with the horizontal seismic
 316 coefficient, the pore-water ratio and the wall inclination (β). Considering the crack formation as a part of the failure

317 mechanism leads to larger required reinforcement strength values than the ones obtained when considering an intact
 318 soil.

319 It is evident that increasing the horizontal seismic coefficient k_h , increases the required reinforcement tensile
 320 strength. Moreover, the pore-water pressure is found to be unfavorable to the reinforced soil wall stability. The presence
 321 of cracks leads to larger required reinforcement strength. In particular, when the value of the pore-water pressure or of
 322 the seismic loading is important, the required reinforcement strength increase is more obvious. Hence, it is critical to
 323 consider these effects when poorly draining cohesive soils are used, as backfill materials, in seismic zones for economic
 324 reasons.

325



326

327

Fig. 5. Required reinforcement strength against seismic coefficient for intact and cracked backfills

328 The reinforcement strength required to prevent the failure of geosynthetic reinforced soil retaining wall, for different
 329 values of horizontal seismic coefficient, pore-water ratio and wall inclination (β) are also presented in Table 1. Two
 330 crack cases are considered. Table 1 presented also the normalized crack depth ξ in case of crack formation as a part of
 331 the failure mechanism. The results showed that the normalized crack depth ξ of the critical failure surface generally
 332 decreased with the increase of β and k_h . However, when the pore-water ratio is high ($r_u = 0.4$), some exceptions
 333 observed.

334

Table 1 Required reinforcement strength and normalized crack depth for different values of r_u and k_h .

r_u	k_h		$\frac{nT_t}{\gamma H^2}$		Normalized crack depth ξ	
			$\beta = 75^\circ$	$\beta = 90^\circ$	$\beta = 75^\circ$	$\beta = 90^\circ$
0	0	No crack	0.025	0.085	-	-
		Crack formation	0.028	0.091	0.241	0.222

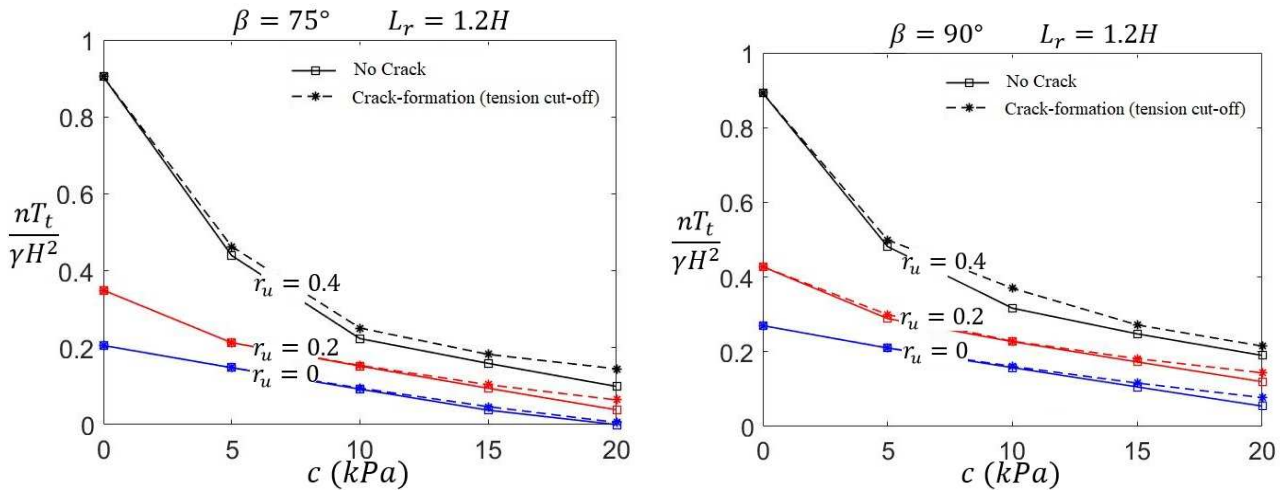
0.05	No crack	0.042	0.108	-	-
	Crack formation	0.048	0.113	0.220	0.207
0.1	No crack	0.064	0.131	-	-
	Crack formation	0.069	0.137	0.204	0.196
0.15	No crack	0.086	0.156	-	-
	Crack formation	0.092	0.162	0.190	0.187
0	No crack	0.079	0.157	-	-
	Crack formation	0.083	0.159	0.321	0.277
0.05	No crack	0.100	0.177	-	-
	Crack formation	0.104	0.180	0.282	0.252
0.1	No crack	0.122	0.199	-	-
	Crack formation	0.127	0.203	0.254	0.232
0.15	No crack	0.146	0.222	-	-
	Crack formation	0.151	0.242	0.230	0.164
0	No crack	0.146	0.243	-	-
	Crack formation	0.150	0.243	0.597	0
0.05	No crack	0.167	0.261	-	-
	Crack formation	0.169	0.263	0.466	0.003
0.1	No crack	0.189	0.279	-	-
	Crack formation	0.199	0.306	0.318	0.350
0.15	No crack	0.234	0.339	-	-
	Crack formation	0.296	0.401	0.510	0.450

335

336 Fig.6 shows the soil cohesion effect on the reinforcement strength required to prevent the reinforced soil wall
337 failure, considering different pore-water coefficients values for a homogeneous backfill soil. The horizontal seismic
338 coefficient is equal to 0.1. The pore pressure coefficient increase leads to a significantly increase of the normalized
339 reinforcement strength. It is clear that the soil cohesion improves wall stability. When the soil cohesion increases, the
340 normalized required reinforcement strength decreases for different values of r_u , for both reinforced earth walls
341 inclinations. The influence of the soil cohesion is more pronounced in the case of a pore-water coefficient r_u equal to
342 0.4. The required reinforcement strength is slightly greater for the crack presence case. The discrepancy between the
343 curves corresponding to the cases of crack formation and no crack is more noticeable when the soil cohesion increases.

344 For the inclined retaining wall with $\beta = 75^\circ$, for a soil cohesion c higher than 19 kPa and a pore-water coefficient
345 r_u equal to zero, the required reinforcement strength which ensure the reinforced soil wall stability is zero. There is no
346 need to reinforced the backfill area with geosynthetic elements.

347



348

349

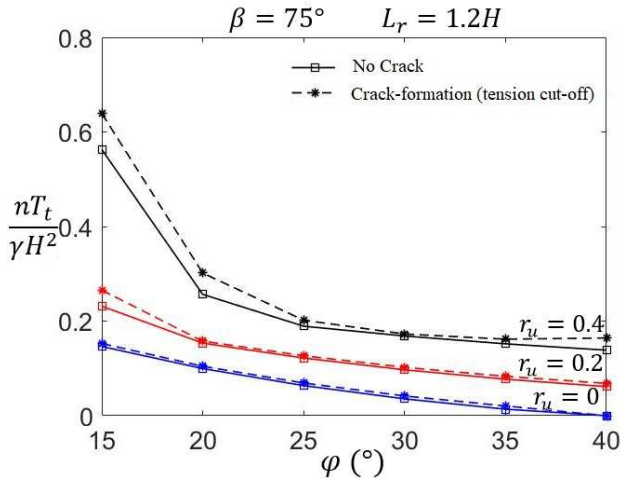
Fig. 6. Required reinforcement strength against soil cohesion for intact and cracked backfill

350

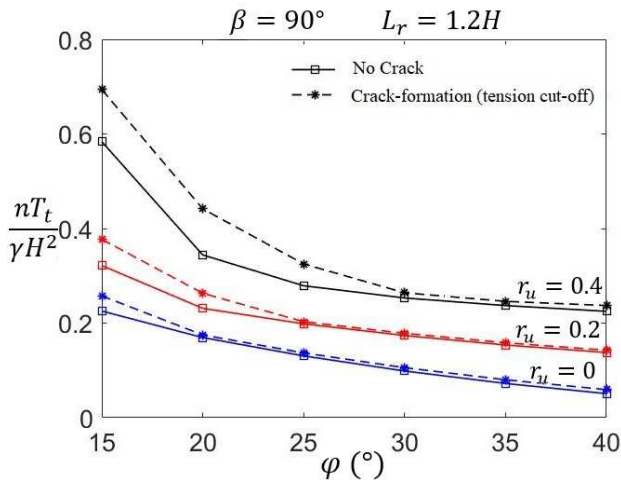
351 The soil friction influence on the tensile strength of the geosynthetic reinforcements used to maintain the reinforced
 352 soil wall stability is presented in Fig. 7 for different pore pressure coefficients. An uniform backfill soil and a horizontal
 353 seismic coefficient equal to 0.1 are considered. It is clear that higher friction angle implies better quality backfills and
 354 therefore, that the required reinforcement strength is higher in case lower friction angle values for both reinforced soil
 355 structures inclinations and different values of r_u , considering or not the presence of cracks. The effect of the soil friction
 356 angle φ increases with the increases of the values of r_u . The required reinforcement strength is slightly greater for the
 357 crack presence case. It is important to note that this difference between the results obtained considering or not the crack
 358 presence decreases when increasing the soil friction angle φ as well as when decreasing the pore-water coefficient r_u
 359 and the wall inclination.

360 For the inclined retaining wall with $\beta = 75^\circ$, the required reinforcement strength that assure the reinforced soil wall
 361 stability is equal to zero for a soil friction angle higher than 37° and a zero pore-water coefficient r_u value.

362



363



364

365

366

Fig. 7. Required reinforcement strength against soil friction angle for intact and cracked backfill

367

7.2 Required reinforcement strength for reinforced non-homogeneous soil retaining walls

368

Most previous studies on the reinforced soil retaining walls stability assume a homogeneous soil. However, soils are non-homogeneous in nature and their properties show spatial variability (Pan and Dias, 2015). This heterogeneity affects the reinforced soil retaining walls stability, hence the importance of its consideration in the design. The conventional kinematic theorem can only be used in cases of homogeneous soils. The discretization-based kinematic analysis method gives the ability to overcome this limitation, and to consider the soil heterogeneity. The variation of the soil strength parameters, the soil friction angle and cohesion, are considered. On the other hand, the soil unit weight γ is considered constant in the whole domain. In this study, for convenience and simplicity, two types of heterogeneity are considered: the soil properties increase linearly with depth and layered backfill soil profile.

376

7.2.1 Linearly increased soil strength profile

377

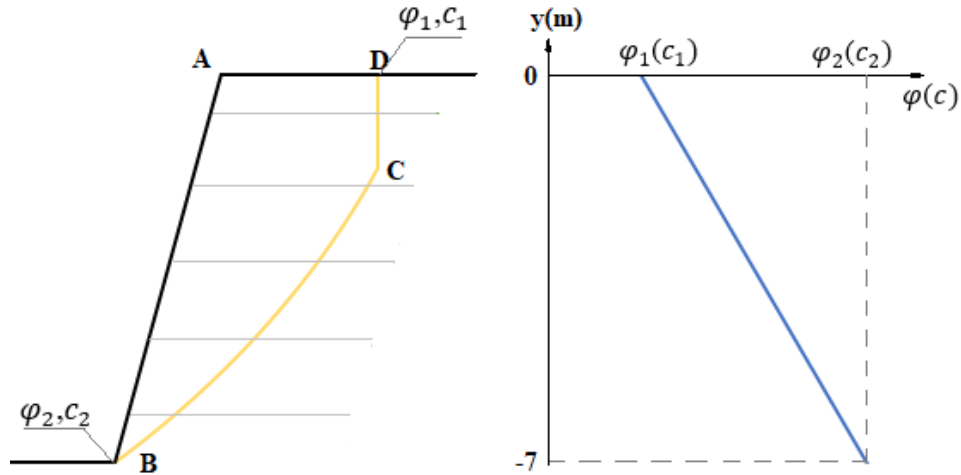
The soil strength parameters are assumed to vary linearly only in the vertical direction (Fig. 8). This means that they are assumed to be constant in the horizontal plane, i.e. at the same depth. The soil unit weight variation is neglected in

378

379 the whole domain. c_1 and φ_1 are respectively the soil cohesion and friction angle at the ground surface, while c_2 and
 380 φ_2 are those at the wall toe level.

381

382



383

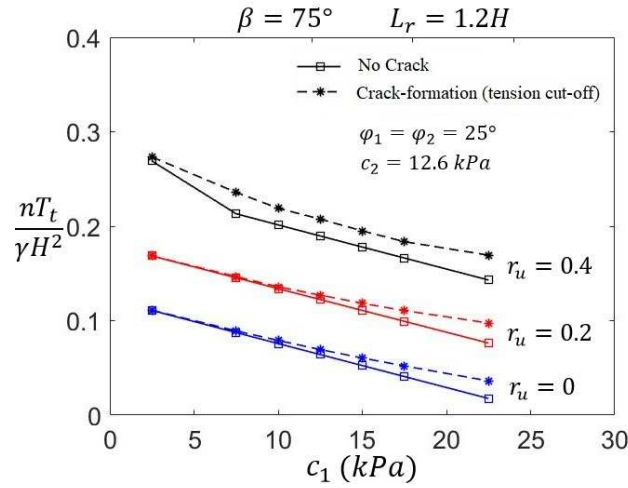
384

Fig.8. Distribution of the soil properties with depth

385 The effect of each soil strength parameters variability is investigated separately. When analyzing the influence of a
 386 parameter, the second one is taken as constant. An inclined reinforced earth wall with $\beta=75^\circ$ is considered. The other
 387 parameters are kept the same as the previous section: $H=7\text{ m}$, $\gamma=18\text{ kN/m}^3$, $\delta\theta=0.01^\circ$, $k_h=0.1$, $\lambda=0.5$, $L_r=1.2\text{ H}$,
 388 $n=10$, $f_0^*=1.2$, $f_1^*=0.6$, $f=1.2$, $V_s=150\text{ m/s}$, $V_p=280.5\text{ m/s}$, and $T=0.3\text{ s}$

389 First, the influence of the soil cohesion variability is investigated. The required normalized reinforcement strength is
 390 plotted against different ground surface soil cohesion values c_1 (Fig. 9). The soil cohesion at the wall toe level is kept
 391 equal to $c_2=12.6\text{ kPa}$. The soil friction angle is considered constant across the whole field $\varphi_1=\varphi_2=25^\circ$.

392 A decrease of the required reinforcement strength is observed when c_1 increases from 2.5 to 22.5 kPa for both
 393 cases of intact or cracked soil. The required reinforcement strength obtained in case of crack formation is higher than
 394 the case of an intact soil. The difference between the two cases is more pronounced for greater values of c_1 . The
 395 required reinforcement strength decreases linearly with c_1 for the case of water-pressure coefficients r_u equals to 0 and
 396 0.2. However, for $r_u = 0.4$, the rate of decrease is greater for c_1 smaller than 7.5 kPa. This can be explained by the
 397 reinforcements pullout failure that occurs in some layers under these conditions.



398

399

Fig. 9. Required reinforcement strength against non-uniform soil cohesion for intact and cracked backfill

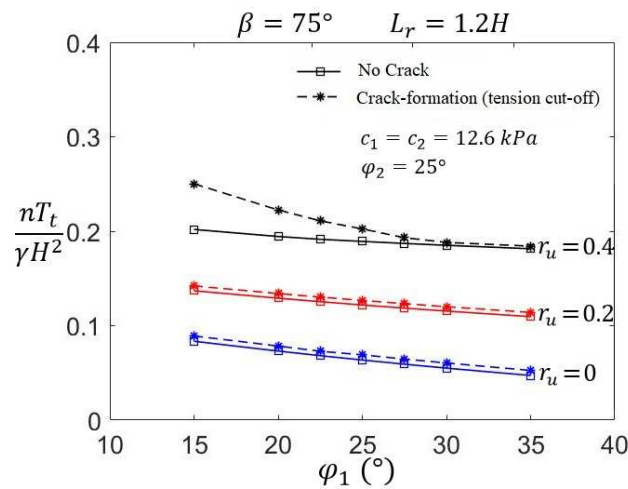
400

The influence of the soil friction angle variability is also investigated apart. The required normalized reinforcement strength is plotted against different ground surface soil friction angles φ_1 (Fig. 10). The soil friction angle at the wall toe level is kept equal to $\varphi_2=25^\circ$. The soil cohesion is considered constant across the whole field $c_1=c_2=12.6\text{ kPa}$.

403

The increase of φ_1 from 15° to 35° decreases slightly the required normalized reinforcement strength and therefore, this increase slightly enhances the reinforced earth wall stability for both intact and cracked soils and different values of r_u . The required reinforcement strength is slightly greater for the crack presence case except the case of pore-water pressure r_u equal to 0.4, and precisely for soil friction angle φ_1 at the wall toe smaller than 25° . Wherein that case, the difference between the intact soil case and the cracked soil one becomes significant, and increases with the soil friction angle φ_1 decrease. This is because the reinforcements pullout failure in some layers in the case of cracked soils.

409



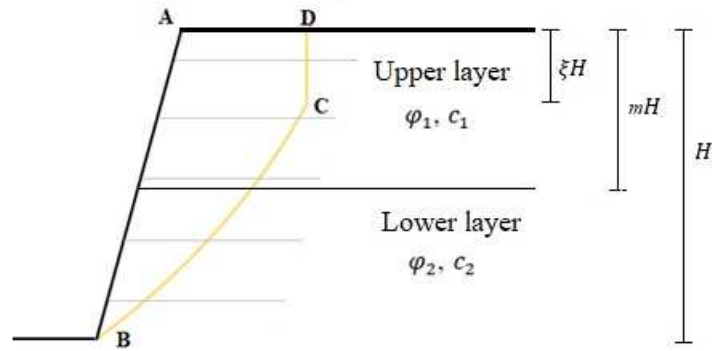
410

411

Fig. 10. Required reinforcement strength against non-uniform soil friction angle for intact and cracked backfill

412 7.2.2 Layered soil profile

413 In most of the real cases, the soil profile is a layered one. In this section, a reinforced soil retaining wall with a
414 stratified backfill composed of two soil layers with different soil strength parameters (see Fig. 11), is analyzed using the
415 developed method. A coefficient m is defined to distinguish the stratified condition as the ratio of the upper layer height
416 to the wall height. The soil strength parameters are φ_1 and c_1 in the upper layer and φ_2 and c_2 in the lower one.

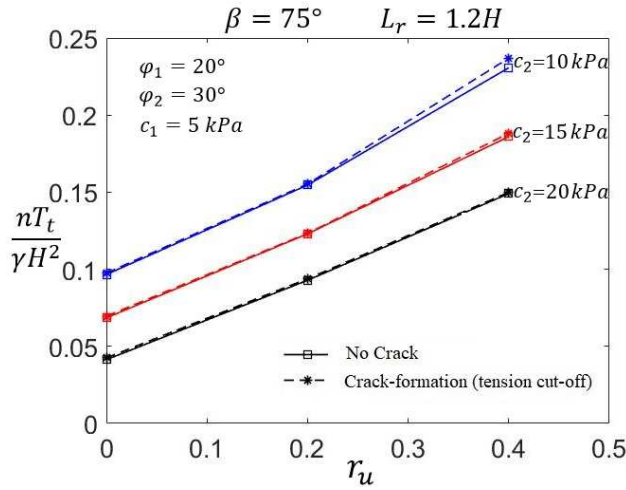


417
418 **Fig. 11.** Heterogeneous backfill with two soil layers

419 The reinforced soil wall considered is inclined with $\beta=75^\circ$ and all the parameters are kept the same as the previous
420 sections except the soil strength parameters. Fig. 12 shows the pore-water pressure coefficient r_u and soil cohesion c_2 of
421 the lower layer influences on the normalized required reinforcement strength. The analysis without the presence of
422 cracks as well as the case of crack formation are both considered. A two-layered backfill required higher reinforcement
423 strength in order to prevent the structure failure when the coefficient r_u increased and when the soil cohesion c_2 in the
424 lower layer decreased.

425 The required reinforcement strength is slightly greater in case of the crack presence in the failure surface. An
426 increase in the lower layer soil cohesion c_2 from 10 to 20 kPa leads to 35.37% and 36.73% reduction of the
427 normalized required reinforcement strength for intact and cracked soil respectively, for a pore-water pressure
428 coefficient equal to 0.4. These reductions become respectively equal to 57.21% and 56.35% for intact and cracked
429 soils when the pore-water pressure does not exist ($r_u = 0$).

430



431

432

Fig. 12. Required reinforcement strength against r_u and soil cohesion c_2 for a two-layered backfill

433

434

435

436

437

Fig. 13 illustrates the influence of the pore-water pressure coefficient r_u and lower layer soil friction angle φ_2 on the normalized required reinforcement strength. The same two crack cases are considered. The stability of the reinforced soil wall is improved when the coefficient r_u decreased and when the soil friction angle φ_2 in the lower layer increased. This is logical since the water has a destabilizing effect and the soil friction angle increase enhances the wall stability by providing an additional resistance.

438

439

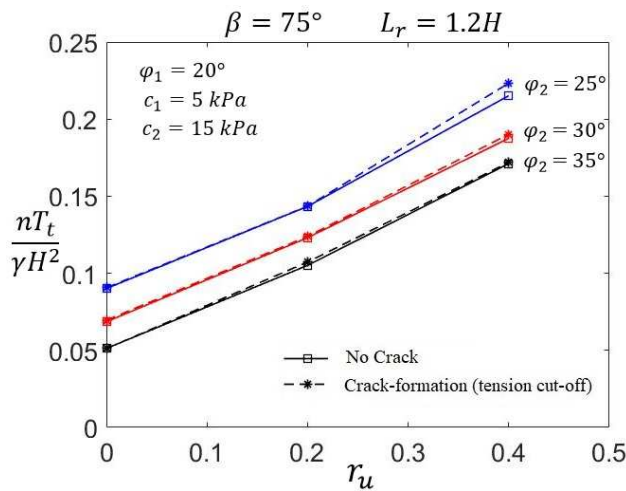
440

441

442

Considering the crack formation through the failure mechanism leads to a higher required reinforcement strength. A decrease in the lower layer soil friction angle φ_2 from 35 to 25° leads to respectively 75.8% and 77.12% of normalized required reinforcement strength increase for intact and cracked soil, for a zero pore-water pressure coefficient. These increases become respectively equal to 25.73% and 29.84% for intact and cracked soil when the pore-water pressure coefficient is equal to 0.4.

443



444

445

Fig. 13. Required reinforcement strength against r_u and soil friction angle φ_2 for a two-layered backfill

446 8 Conclusion

447 This paper investigates the seismic internal stability of geosynthetic reinforced saturated soil wall considering soil
448 cracks, using the kinematic theorem of limit analysis combined with the discretization technique. The results are
449 presented in terms of required reinforcement strength that prevent wall failure. The discretization technique consists to
450 generate the rotational sliding surface of the reinforced soil wall point by point based on the associated flow rule. This
451 method represents a suitable tool to overcome the limitations of the conventional upper bound limit analysis method. It
452 gives the ability to easily integrate the soil spatial variability properties for nonhomogeneous or multi-layered soils. In
453 addition of the benefits of considering the soil heterogeneity, it allows the implementation of the pseudo-dynamic
454 approach which takes into account the aspects neglected by the pseudo-static approach adopted in the conventional
455 kinematic analysis. The effect of the buoyancy forces and seepage forces are considered. It is included as an additional
456 external force in the limit analysis upper bound method.

457 In order to validate the proposed approach, the obtained results are verified by comparison with those obtained by
458 Abd and Utili (2017), who evaluated the reinforced slopes stability, using the conventional upper bound approach of
459 limit analysis. Pre-existing crack as well as crack formation through the collapse mechanism are considered without
460 consideration of the seismic loading. A good consistency between the two approaches proves the developed method
461 effectiveness.

462 The effects of the crack presence, seismic loading and the soil strength parameters on the required reinforcement
463 strengths are assessed. Three scenarios are considered for the backfill soil strength parameters, a homogeneous soil,
464 non-homogeneous soil with a linearly increased strength parameters or a layered backfill.

465 The consideration of the crack formation is found to have a destabilizing effect on the reinforced soil retaining walls
466 stability. This is more pronounced for lower soil friction angle values, greater values of soil cohesion and pore water
467 coefficient.

468 The pore water pressure has also a negative effect on these structures. In addition, the required reinforcement
469 strength is highly dependent on the soil strength parameters. The soil friction angle and cohesion enhance the reinforced
470 soil wall stability.

471 The discretization-based kinematic analysis have shown its effectiveness for the seismic internal stability analysis of
472 reinforced saturated soil retaining walls with crack presence. The key advantage of this method is its capacity to deal
473 with multi-layered or nonhomogeneous soil profiles. In addition, it allows the implementation of the pseudo-dynamic
474 approach which gives the benefits of considering the dynamic characteristic of the seismic loading.

475 **Numerical calculations or physical models will be necessary to evaluate the reliability of the developed method in**
476 **this paper.**

477 **References**

- 478 Abd, A.H., Utili, S., 2017. Design of geosynthetic-reinforced slopes in cohesive backfills. *Geotext. Geomembranes* 45,
479 627–641. <https://doi.org/10.1016/j.geotexmem.2017.08.004>
- 480 Ahmad, S.M., Choudhury, D., 2008. Pseudo-dynamic approach of seismic design for waterfront reinforced soil-wall.
481 *Geotext. Geomembranes* 26, 291–301. <https://doi.org/10.1016/j.geotexmem.2007.12.004>
- 482 Alhadj Chehade, H., Dias, D., Sadek, M., Jenck, O., Hage Chehade, F., 2021. Pseudo-static Analysis of Reinforced
483 Earth Retaining Walls. *Acta Geotech.* 2. <https://doi.org/10.1007/s11440-021-01148-2>
- 484 Alhadj Chehade, H., Dias, D., Sadek, M., Jenck, O., Hage Chehade, F., 2020. Upper bound seismic limit analysis of
485 geosynthetic-reinforced unsaturated soil walls. *Geotext. Geomembranes*.
486 <https://doi.org/10.1016/j.geotexmem.2020.02.001>
- 487 Alhadj Chehade, H., Dias, D., Sadek, M., Jenck, O., Hage Chehade, F., 2019. Seismic analysis of geosynthetic-
488 reinforced retaining wall in cohesive soils. *Geotext. Geomembranes* 47, 315–326.
489 <https://doi.org/10.1016/j.geotexmem.2019.02.003>
- 490 Baker, R., 1981. Tensile strength, tension cracks, and stability of slopes. *Soils Found.* 21, 1–17.
491 https://doi.org/10.3208/sandf1972.21.2_1
- 492 Baker, R., Leshchinsky, D., 2003. Spatial distribution of safety factors: Cohesive vertical cut. *Int. J. Numer. Anal.*
493 *Methods Geomech.* 27, 1057–1078. <https://doi.org/10.1002/nag.312>
- 494 Baker, R., Leshchinsky, D., 2001. Spatial distribution of safety factors. *J. Geotech. Geoenvironmental Eng.* 127, 135–
495 145. [https://doi.org/10.1061/\(ASCE\)1090-0241\(2001\)127:2\(135\)](https://doi.org/10.1061/(ASCE)1090-0241(2001)127:2(135))
- 496 Basha, B.M., Sivakumar Babu, G.L., 2011. Seismic reliability assessment of internal stability of reinforced soil walls
497 using the pseudo-dynamic method. *Geosynth. Int.* 18, 221–241. <https://doi.org/10.1680/gein.2011.18.5.221>
- 498 Chen, W.-F., Giger, M.W., Fang, H.Y., 1969. On the limit analysis of stability of slopes. *Soils Found.* 9, 23–32.
499 https://doi.org/10.3208/sandf1960.9.4_23
- 500 Choudhury, D., Nimbalkar, S.S., 2006. Pseudo-dynamic approach of seismic active earth pressure behind retaining
501 wall. *Geotech. Geol. Eng.* 24, 1103–1113. <https://doi.org/10.1007/s10706-005-1134-x>
- 502 Chowdhury, R.N., Zhang, S., 1991. Tension cracks and slope failure, in: *Proceedings of the International Conference:*
503 *Slope Stability Engineering, Developments and Applications.* Thomas Telford, London, pp. 27–32.
504 <https://doi.org/10.1680/ssedaa.16606.0005>
- 505 Guler, E., Hamderi, M., Demirkan, M.M., 2007. Numerical analysis of reinforced soil-retaining wall structures with
506 cohesive and granular backfills. *Geosynth. Int.* 14, 330–345. <https://doi.org/10.1680/gein.2007.14.6.330>
- 507 Guo, X., Dias, D., Carvajal, C., Peyras, L., Breul, P., 2018. Reliability analysis of embankment dam sliding stability

508 using the sparse polynomial chaos expansion. *Eng. Struct.* 174, 295–307.
509 <https://doi.org/10.1016/j.engstruct.2018.07.053>

510 Hu, Y., Zhang, G., Zhang, J.-M., Lee, C.F., 2010. Centrifuge modeling of geotextile-reinforced cohesive slopes.
511 *Geotext. Geomembranes* 28, 12–22. <https://doi.org/10.1016/j.geotexmem.2009.09.001>

512 Koerner, R.M., Koerner, G.R., 2018. An extended data base and recommendations regarding 320 failed geosynthetic
513 reinforced mechanically stabilized earth (MSE) walls. *Geotext. Geomembranes* 46, 904–912.
514 <https://doi.org/10.1016/j.geotexmem.2018.07.013>

515 Ling, H.I., Leshchinsky, D., Chou, N.S., 2001. Post-earthquake investigation on several geosynthetic-reinforced soil
516 retaining walls and slopes during the ji-ji earthquake of Taiwan. *Soil Dyn. Earthq. Eng.* 21, 297–313.
517 [https://doi.org/10.1016/S0267-7261\(01\)00011-2](https://doi.org/10.1016/S0267-7261(01)00011-2)

518 Michalowski, R.L., 2013. Stability assessment of slopes with cracks using limit analysis. *Can. Geotech. J.* 50, 1011–
519 1021. <https://doi.org/10.1139/cgj-2012-0448>.

520 Mollon, G., Dias, D., Soubra, A.-H., 2011. Rotational failure mechanisms for the face stability analysis of tunnels
521 driven by a pressurized shield. *Int. J. Numer. Anal. Methods Geomech.* 35, 1363–1388.

522 Nimbalkar, S.S., Choudhury, D., Mandal, J.N., 2006. Seismic stability of reinforced-soil wall by pseudo-dynamic
523 method. *Geosynth. Int.* 13, 111–119. <https://doi.org/10.1680/gein.2006.13.3.111>

524 Pan, Q., Dias, D., 2015. Face Stability Analysis for a Shield-Driven Tunnel in Anisotropic and Nonhomogeneous Soils
525 by the Kinematical Approach. *Int. J. Geomech.* 16, 04015076. [https://doi.org/10.1061/\(ASCE\)GM.1943-5622.0000569](https://doi.org/10.1061/(ASCE)GM.1943-5622.0000569)

526

527 Porbaha, A., Goodings, D., 1996. Centrifuge modeling of geotextile-reinforced cohesive soil retaining walls. *J.*
528 *Geotech. Eng.* 122, 840–848. [https://doi.org/10.1061/\(ASCE\)0733-9410\(1996\)122:10\(840\)](https://doi.org/10.1061/(ASCE)0733-9410(1996)122:10(840))

529 Qin, C.-B., Chian, S.C., 2019. Pseudo-static/dynamic solutions of required reinforcement force for steep slopes using
530 discretization-based kinematic analysis. *J. Rock Mech. Geotech. Eng.* 11, 289–299.
531 <https://doi.org/10.1016/j.jrmge.2018.10.002>

532 Qin, C.-B., Chian, S.C., 2018. Bearing capacity analysis of a saturated non-uniform soil slope with discretization-based
533 kinematic analysis. *Comput. Geotech.* 96, 246–257. <https://doi.org/10.1016/j.compgeo.2017.11.003>

534 Qin, C.-B., Chian, S.C., 2017. Kinematic analysis of seismic slope stability with a discretisation technique and pseudo-
535 dynamic approach: a new perspective. *Géotechnique* 68, 492–503. <https://doi.org/10.1680/jgeot.16.P.200>

536 Riccio, M., Ehrlich, M., Dias, D., 2014. Field monitoring and analyses of the response of a block-faced geogrid wall
537 using fine-grained tropical soils. *Geotext. Geomembranes* 42, 127–138.
538 <https://doi.org/10.1016/j.geotexmem.2014.01.006>

539 Steedman, R.S., Zeng, X., 1990. The influence of phase on the calculation of pseudo-static earth pressure on a retaining

540 wall. *Géotechnique* 40, 103–112. <https://doi.org/10.1680/geot.1990.40.1.103>

541 Sun, Z., Li, J., Pan, Q., Dias, D., Li, S., Hou, C., 2018. Discrete Kinematic Mechanism for Nonhomogeneous Slopes
542 and Its Application. *Int. J. Geomech.* 18, 04018171. [https://doi.org/10.1061/\(asce\)gm.1943-5622.0001303](https://doi.org/10.1061/(asce)gm.1943-5622.0001303)

543 Utili, S., 2013. Investigation by limit analysis on the stability of slopes with cracks. *Géotechnique* 63, 140–154.
544 <https://doi.org/10.1680/geot.11.P.068>

545 Utili, S., Abd, A.H., 2016. On the stability of fissured slopes subject to seismic action. *Int. J. Numer. Anal. Methods*
546 *Geomech.* 40, 785–806. <https://doi.org/10.1002/nag.2498>

547 Viratjandr, C., Michalowski, R.L., 2006. Limit analysis of submerged slopes subjected to water drawdown. *Can.*
548 *Geotech. J.* 43, 802–814. <https://doi.org/10.1139/T06-042>

549 Zhao, L.H., Cheng, X., Zhang, Y., Li, L., Li, D.J., 2016. Stability analysis of seismic slopes with cracks. *Comput.*
550 *Geotech.* 77, 77–90. <https://doi.org/10.1016/j.compgeo.2016.04.007>

551

552